RSC Advances

ROYAL SOCIETY OF CHEMISTRY

www.rsc.org/advances

Preparation of Magnetic Molecularly Imprinted Polymer Beads and Their Recognition for Baicalein

Song Wang,[a,b] Huitong Si[a], Bing Wang[*,a] Juanjuan Shan,[a] and Xinlin Yang[*b]

a) State Key Laboratory of Hollow Fiber Membrane Materials and Processes (Tianjin Polytechnic University), School of Materials Science and Engineering, Tianjin Polytechnic University, Tianjin 300387, P. R. China

b) Key Laboratory of Functional Polymer Materials, Ministry of Education, Institute of Polymer Chemistry, Collaborative Innovation Center of Chemical Science and Engineering (Tianjin), Nankai University, Tianjin 300071, P. R. China

Abstract

Magnetite-β-cyclodextrin@poly(ethyleneglycol dimethacrylate-*co*-methacrylic acid) core-shell microspheres imprinted with baicalein (Fe_3O_4-β-CD@MIPs) were synthesized by ultrasonic assisted precipitation polymerization (UAPP) using methacrylic acid (MAA) as functional monomer and EGDMA as crosslinker in presence of Fe_3O_4-β-CD nanoparticles as template and baicalein (BAI) as imprinting molecule. The structure, morphology and magnetic property of the resultant Fe_3O_4-β-CD@MIPs have been systematically characterized by the transmission electron microscopy (TEM), Fourier-transform infrared spectra (FT-IR), vibrating sample magnetometry (VSM), and thermogravimetric analysis (TGA). The unique recognition ability of Fe_3O_4-β-CD@MIPs for BAI was evaluated by the adsorption experiments via comparing those of Fe_3O_4@MIPs and Fe_3O_4-β-CD@NIPs non-imprinted nanoparticles.

Keywords: Molecularly imprinted microsphere; Baicalein; β-Cyclodextrin; Magnetic nanoparticles; Precipitation polymerization.

Introduction

Baicalein (BAI) is one of the main active ingredients of the dry root of Chinese medicinal plant named Scutellaria Baicalensis Geogri (SBG) [1]. BAI can be considered as one of the most promising chemo-preventive and effective agents for cancer, which is mainly extracted from SBG [2]. It may be found the potential applications to induce HIV apoptosis [3], avoid liver poisoning [4] and inhibit cell proliferation [5] via *in vitro* studies based on its wide range of biological effects and low toxicity.

It is well-known that the pharmacologically active compounds in herbal plants have low concentrations and complex chemical constituents. It is essential to develop an effective technique for quantitative determination, recognition and purification of BAI molecules from those components in SBG. Several analytical methods, such as heat refluxing [6] and adsorption chromatography separation [7], have been successfully utilized for the quantitative determination of BAI. However, these analytical procedures are always time-consuming with a high cost. It would be a feasible way to solve these problems via utilization of a solid adsorbent with specific recognition property, which has a great potential value for the study of biological process as well as its in-depth application. From these aspects, it is a superior choice to employ molecularly imprinted materials with specific adsorption.

Molecularly imprinted polymers (MIPs) have attracted much attention for their outstanding advantages, including the unique adsorption performances, chemical resistance, mechanical stability, relative facile and low-cost of the preparation [8]. As a result, MIPs have been widely used in many areas, such as adsorbents [9], membranes [10], solid-phase extraction [11], biosensors [12], isolation [13], chromatography stationary phase for efficient separation and specific recognition [14]. The outstanding performance of MIPs depends on the shape memory towards the template via hydrogen bonding, and hydrophobic interactions. The MIPs has been manufactured in various morphologies, including membrane, microspheres. Recently, the core-shell magnetic MIPs have attracted a large of concern. It would be a promising solution to fully utilize the advantages of the magnetic NPs for efficient separation and enrichment, and recognition of the template molecule via a simple imposed magnetic field from a complex system. MIPs coatings on magnetic Fe_3O_4 NPs with a core-shell structure (Fe_3O_4@BHb-MIPs) have been synthesized via combination of surface imprinting and sol-gel techniques for recognition and enrichment of proteins with accessible recognition sites, high capacity and favorable selectivity [15]. The magnetic indole-3-acetic acid (IAA) imprinted polymer beads have been synthesized by suspension polymerization of 4-vinylpyridine (4-VPy) and trimethylolpropane trimethacrylate (Trim) crosslinker having an improved recognition ability to IAA with the aid of a silanized β-CD arm [16].

In recent years, β-Cyclodextrin (β-CD) has been widely utilized to recognize target molecule of compatible size based on its hydrophobic cavity together with a hydrophilic external surface [17]. Therefore, it would be a promising solution through preparation of MIPs with β-CD to contain hydrophobic and hydrophilic functionalities in a single material. The imprinting efficiency of traditional MIPs with individual functional monomer, such as MAA, 4-VP, will be improved.

In the process of synthesis of MIPs, there are many methods have been used, such as bulk polymerization [18], suspension polymerization [19], emulsion polymerization [20], precipitation polymerization [21]. In recent years, precipitation polymerization has been developed as a heterogeneous polymerization technique for the synthesis of polymer micro-/nanospheres with uniform size, shape and various functionalities in absence of any added surfactant or stabilizer [22]. Unfortunately, the abhorrent long polymerization time is inevitable. In order to resolve the problem, the ultrasound-assisted preparation polymerization [23] was utilized. As a result, the

polymerization time was greatly shorted. Herein, the magnetic MIP beads with a core-shell structure has been designed, synthesized by the microwave-assisted precipitation polymerization of methacrylic acid functional monomer (MAA), ethyleneglycol dimethacrylate (EGDMA) crosslinker in presence of the silanized β-CD arm coated magnetite nanoparticle (Fe_3O_4) as a template. The mechanism for the construction of Fe_3O_4-β-CD@BAI-MIPs core-shell microspheres have been elucidated and the primary recognition of the MIPs for baicalein with a facile recovery via a magnetic separation process. The imprinting efficiency between individual functional monomer and assisted β-CD for conventional MIPs has been discussed.

Experimental

Materials. Baicalein (BAI) and quercetin (Qu) were purchased from Ciyuan Biotechnology Co Ltd (Shaanxi, Chin). Chloramphenoicol (CAP) was bought from Wuhan Pharmaceutical Chemical Co Ltd (Wuhan, China). Methacrylic acid (MAA), dimethylsulfoxide (DMSO), acetonitrile (AN), methanol, acetic acid, ethanol and dimethyl formamide (DMF) were purchased from Tianjin Kermal Chemical Reagent Co Ltd (Tianjin, China). *N,N*' Azo-bis-isobutyronitrile (AIBN) and β-cyclodextrin (β-CD) were provided by Damao Reagent Plant (Tianjin, China). Ethyleneglycol dimethacrylate (EGDMA) and glycidoxypropyltrimethoxysilane (GPTMS) were afforded from Corel Chemical Plant (Shanghai, China). Ferric chloride hexahydrate ($FeCl_3 \cdot 6H_2O$), ferrous chloride tetrahydrate ($FeCl_2 \cdot 4H_2O$), sodium hydroxide and sodium hydride were bought from Tianjin Guangfu Fine Chemical Research Institute (Tianjin, China). Polyethylene glycol (PEG M_w=6000) was obtained from Tianjin Tiantai Chemical Reagents (Tianjin, China). MAA was purified by vacuum distillation and AIBN was recrystallized in methanol before utilization.

Preparation the PEG-modified Fe_3O_4 nanoparticles

The Fe_3O_4 magnetic nanoparticles were first prepared by the co-precipitation technique according to the literature [24, 25] as following. Briefly, 2.7 g $FeCl_3 \cdot 6H_2O$ (1.0 mmol Fe(III)) and 1.0 g $FeCl_2 \cdot 4H_2O$ (0.5 mmol Fe(II)) were dissolved in 150 mL of de-ionized water under nitrogen with mild stirring for 10 min. Then the mixture was heated to 50 °C and 20 mL of sodium hydroxide aqueous solution was added dropwise into the reaction system with vigorous mechanical stirring. After 30 min, the reaction was heated and maintained at 90 °C for 60 min. After the reaction, the black precipitate was collected with the aid of the outer magnetic field and washed several times by ethanol and distilled water successively. Finally, the resultant Fe_3O_4

nanoparticles (500 mg) were modified with PEG aqueous solution (1.0 g, 25 wt% in distilled water) and then mixed with ultra-sonication as magnetic ferro-fluid (Fe_3O_4-PEG) for further utilization.

Synthesis of silylated β-CD

1.0 g of β-CD was dissolved in 30.0 mL of anhydrous DMF solution, 0.1 g of NaH was added into the mixture with vigorous stirring for 90 min. After the reaction, the excess NaH was rapidly filtered. Then 0.5 mL of GPTMS was added into the reaction solution dropwise. The silanation of β-CD was performed at 80 °C for 15 h. The resultant precipitate was washed with anhydrous DMF, methanol and acetone sequentially and dried at 100 °C in a vacuum oven till constant weight.

Synthesis of Fe_3O_4-β-CD@BAI-MIPs

The DMF (50 mL) and NaOH solution (25wt%, 2 mL) were successively added into the above resultant materials. Then, the mixture solution was left to react for 12 h with vigorous stirring. The target products (Fe_3O_4@PEG/β-CD) were separated via an external magnetic field, and rinsed sequentially with DMF, water, and methanol. After drying under vacuum at 50 °C, 0.27 g (1.0 mmol) of BAI, and 0.17 g (2.0 mmol) of MAA were dissolved in 15 mL of anhydrous DMF and agitated by rolling the bottles in a horizontal position at approximately 140 rpm on an SHA-B shaker for 12 h. Then 0.80 g (4.02 mmol) of EGDMA crosslinker, 20 mg (2wt%, relative to the monomer and crosslinker) of AIBN initiator were dispersed in 100 mL of DMF/deionized water (8/2, V/V) and added into the above mixture solution. Afterwards, the precipitation polymerization was performed at 60 °C with an ultrasonic irradiation for 6 h. After the polymerization, the resultant Fe_3O_4-β-CD@BAI-MIPs was collected via utilization of an applied magnetic field. The BAI templates were selectively removed from the Fe_3O_4-β-CD@BAI-MIPs by a Soxhlet extraction technique with a mixture solvent of methanol and acetic acid (8/2, V/V) as eluant till absence of BAI molecules in the eluent, which was determined by UV spectrometry with the absorption peak at 275 nm. The resultant nanoparticles (Fe_3O_4-β-CD@MIPs) were finally rinsed in ethanol to remove the residual acetic acid and dried at 60 °C till constant weight in a vacuum oven before use.

For comparisons, Fe_3O_4@MIPs in absence of the β-CD arm and Fe_3O_4-β-CD@non-imprinted polymers without BAI template (Fe_3O_4-β-CD@NIPs) were also prepared for evaluation of the imprinting efficiency.

The Adsorption experiments

To investigate the adsorption capacity of the resultant functional polymer beads, batch rebinding experiments were implemented as following. 50 mg of the resultant polymer beads, including Fe_3O_4@MIPs, Fe_3O_4-β-CD@NIPs and Fe_3O_4-β-CD@MIPs, were suspended in 5 mL of methanol solution with various BAI concentrations (0-5.0 mmol/L). The suspension was gently agitated by shaking the bottles in a horizontal position at around 150 rpm on a SHA-B shaker at room temperature for 20 h. These polymer beads adsorbed with BAI molecules were separated from the suspension with the aid of an external magnetic field. The concentration of the BAI in the supernatant was detected by UV spectroscopy with the absorption peak at 275 nm. The average adsorption capacity Q (μmol/g) of BAI was repeatedly calculated according to the formula:

$$Q=(C_0-C_t)*V/M \quad (1)$$

where, C_0 (mmol/L) is the initial concentration of BAI, C_t (mmol/L) is the final concentration of BAI after adsorption, V (mL) is the volume of the solution, M (g) is the mass of the polymers.

Based on the above experiment, the dynamic adsorption experiment was implemented. The 50 mg of resultant beads were suspended in 5 mL 2 mmol/L BAI methanol solution. After different adsorption time (5-210 min), the concentration of BAI in the supernatant was detected as same as isothermal adsorption.

Selectivity adsorption experiments

The selectivity test of the above mentioned beads was performed between BAI and the structurally similar compound quercetin (Qu) as well as dissimilar compound chloramphenoicol (CAP). The resultant Fe_3O_4-β-CD@MIPs beads (50 mg) were placed in 6.0 mL the methanol solutions containing 2mL 2 mmol/L of BAI, Qu and CAP, respectively. The adsorption of resultant beads for BAI was performed with mild rolling for 20 h on a SHA-B shaker. After the polymer beads adsorbed with the different molecules were separated from the system under an extra magnetic field, the concentrations of the residual BAI, Qu, and CAP in the solution were measured by UV-vis spectrometry with the determination peaks at 275, 256, 272 nm, respectively.

Calculation of the selectivity adsorption

The static distribution co-efficient index (K_d), selectivity factor (a) and imprinting efficiency (b) were calculated by the following formulae.

$$K_d=C_p/C_s \quad (2)$$

$$a=K_{d(BAI)}/K_{d(reference)} \ (Reference=Qu,CAP) \quad (3)$$

$$\beta=Q_m/Q_n \quad (4)$$

where, C_p (mmol/L) is the initial concentration of adsorbed solution; C_s (mmol/L) is the residual BAI, Qu and CAP concentrations in the solution; $K_{d(BAI)}$ and $K_{d(reference)}$ are the static distribution co-efficient indexes of the BAI template and references of Qu and CAP molecules; Q_m and Q_n represent the adsorption capacities of Fe_3O_4-β-CD@MIPs and Fe_3O_4-β-CD@NIPs, respectively.

Characterization

The morphologies of the nanoparticles were determined by Field emission scanning electron microscopy (FESEM) on S-450 FESEM microscope and transmission electron microscopy (TEM) on an H-7650 TEM microscope (Hitachi, Japan).

The Fourier infrared spectra (FT-IR) were recorded on a TENSOR-37 spectrometer (Brucker, Germany) ranging from 4000 to 400 cm^{-1} with a potassium bromide pellet.

Thermogravimetric analysis (TGA) was performed on a SAT 409 PC (Netzsch, Germany) via heating from room temperature till 800 ˚C with a rate of 15 ˚C /min under a nitrogen flow.

The magnetic property of the nanoparticle was measured with a VSM (LDJ 9600-1, America) at room temperature.

The concentrations of BAI, Qu and CAP were determined by UV-vis spectra on a UV spectrometer (Tu-1901, China).

The silica content of silylated β-CD was measured with Inductively Coupled Plasma (ICP, JY/ACTIVA-M, France)

Results and Discussion

The magnetic BAI molecularly imprinted polymer beads with a silylated β-CD arm coated PEGylated magnetite (Fe_3O_4-β-CD@BAI-MIPs) were designed and prepared as shown in Scheme 1. The whole procedure for this synthesis mainly involved three steps: i) Preparation of PEGylated magnetite nanoparticles; ii) Preparation of silylated β-CD; iii) Preparation of Fe_3O_4-β-CD@BAI-MIPs via the ultra-sonication assisted precipitation polymerization of the

functional super-monomer MAA-preassembled with the BAI endorsed with the silylated β-CD and the EGDMA crosslinker in presence of the PEGylated magnetite nanoparticle as core. The recognition cavities of the resultant Fe_3O_4-β-CD@MIPs for BAI were afforded by a Soxhlet extraction to selectively remove the imprinted BAI molecules.

Scheme 1

The Mechanism for the Synthesis of Fe_3O_4-β-CD@BAI-MIPs

The magnetic indole-3-acetic acid imprinted polymer beads with β-CD as a functional arm have been successfully synthesized by a microwave heating initiated polymerization and their application has been investigated for trace analysis of auxins in plant tissues [16]. However, the mechanism for the synthesis has not been clearly stated in this work. In our work, the mechanism for the synthesis of Fe_3O_4-β-CD@BAI-MIPs has been described systematically as following.

The magnetite (Fe_3O_4) nanoparticles were prepared by the chemical co-precipitation of Fe(III)/Fe(II) (2/1 in molar ratio) cations in a basic solution (1.0 M NaOH) at 60 °C via a sol-gel process. These magnetite nanoparticles were prone to aggregate in the solvent and during the drying process due to the high specific surface area and strong interparticle interaction. This was confirmed by the FESEM micrograph in Figure 1A with presence of the agglomerate consisting of several magnetite nanoparticles with the average diameter of 10 nm. The formation of the PEGylated Fe_3O_4 nanoparticles not only improved the stability of the composite nanoparticles as shown by the SEM and TEM micrograph in Figure 1B, but also endowed the hydrophilicity and the hydroxyl groups on the surface for the further functionalization and modification of the resultant magnetic nanoparticles [25]. The mass ratio of the PEG components in the PEGylated magnetite nanoparticles was as high as 22% determined by TGA as shown in Figure 5b.

Figure 1

The molecularly imprinted polymers (MIPs) have the special recognition performance based on the specific interaction/reaction between the functional monomer and the template molecule. Therefore, the selection of functional monomer was the most important aspect to achieve a good imprinting efficiency for the MIPs. However, the imprinting efficiency of the traditional MIPs with a simple monomer system is not satisfactory enough for recognition after the selective removal of the template molecule. Herein, the β-CD, as a functional bridge between the BAI molecule and the magnetite core, was introduced to improve the imprinting efficiency during

the recognition. The natural β-CD has certain limitation in practical application [26], such as poor water-solubility, the lesser effective functional sites. In order to improve the compatibility of β-CD, the GPTMS was used to modify the β-CD molecule [27]. The silylated β-CD was prepared via the inter-molecular condensation of the hydroxyl groups on the hydrophilic external surface of β-CD and the methoxy groups of GPTMS with presence of sodium hydride as shown in Scheme 1. The silica content in the silylated β-CD was 6.9% determined by ICP, which was consistent with the theoretical value of 7.7% according to the chemical structure in Scheme 1. The incorporation of the reactive methylsilane group via this modification provided the possibility for silylated β-CD as a functional bridge between the PEGylated magnetite core and the BAI imprinted polymer shell as shown in Scheme 1.

To elucidate the mechanism of the precipitation polymerization and the role of β-CD for the resultant Fe_3O_4-β-CD@BAI-MIPs, the UV-spectra have been carefully and systematically investigated for BAI, MAA/BAI, BAI/β-CD, and MAA/BAI/β-CD in DMF solutions as shown in Figure 2. The UV-spectrum of BAI in DMF has two peaks at 275 and 323 nm, which may be attributed to the hydrophilic cinnamoyl group and the hydrophobic benzoyl group, respectively. The UV-vis spectra of MAA/BAI with different ratios in DMF were illustrated in Figure 2A. It indicated that the peak at 323 nm was gradually weakened with the molar ratio of MAA/BAI increasing from 0/1 till 4/1, while the peak intensity at 275 nm was weakened from 1.33 to 1.23 at presence of MAA. According to the structure of BAI and the changes in the UV spectrum, we deduced that there was a strong hydrogen-bonding interaction between the carboxyl groups of MAA and the hydroxyl groups in BAI molecule as the form of a structure as illustrated in Scheme 1(iii). After the formation of hydrogen-bonding, the density of electron clouds decreased, the π-electron mobility increased, and a lower energy was just required for the transition of electronic energy levels. Consequently, the significant weakening of the spectrum of band was happened. In the Figure 1A, there was an isoabsorptive point at 350 nm. It revealed that the two coordination interaction between BAI and MAA was formed in the process of self-assembly. Figure 2B showed the UV-spectra of BAI/silylated β-CD in DMF with different ratios ranging from 1/0 to 1/4 in molar ratio. It demonstrated that the peak at 323 nm was considerably red-shifted from 323 to 329 nm with the decreasing the ratio of BAI/silylated β-CD from 1/0 to 1/4, while the peak at 275 nm slightly changed. These red-shifts may be originated from the efficient interaction between the

hydrophobic benzoyl group and hydrophobic cavity of β-CD as described in Scheme 1(iii), which reduced the energy gap for the π-π* transition to arise a better stabilization of excitons. With the BAI/silylated β-CD (1/1) as an example, the influence of the MAA on the UV-vis spectra were determined via addition of different amounts of MAA functional monomers as shown in Figure 2C. For the MAA/BAI/silylated β-CD tri-component systems, both the peaks at 283 and 322 nm of the UV-vis spectra were red-shifted. Addition of more and more MAA in this tri-component system had a more significant influence on the absorption peak at 322 nm in UV-vis spectra as observed in Figure 2C, which attributed to the hydrogen-bonding interaction between MAA and BAI/β-CD complex. The UV-vis peak at 322 nm almost disappeared, which may be due to the formation of a core-corona micelle for MAA-BAI/silylated (7:1:1) tri-layer system. In such a case, the hydrophobic part may be located inside the micelle as core, which was shielded by the hydrophilic core during UV-vis irradiation. All these results demonstrated that the pre-assembled MAA/BAI/silylated β-CD super-monomers were formed as shown in Scheme 1(iii) via the strong hydrogen-bonding interaction between the MAA group and the phenol group of BAI together with the efficient hydrophobic interaction between the phenyl group of BAI and the hydrophobic cavity of β-CD, which would facilitate the precipitation polymerization and the improvement in recognition property of the Fe_3O_4-β-CD@BAI-MIPs.

Figure 2

The MAA monomer, silylated β-CD, and BAI were mixed in DMF with BAI/ β-CD/MAA molar ratio of 1:1:2 in a round bottom flask with mild agitation on a SHA-B shaker overnight to form a super-MAA monomer. The Fe_3O_4-β-CD@BAI-MIPs was synthesized by precipitation polymerization of the super-MAA as functional monomer, EGDMA as crosslinker, in presence of PEGylated nanoparticles as core with the aid of ultra-sonic irradiation in DMF/deionized water solvent. The FESEM micrograph of the resultant Fe_3O_4-β-CD@BAI-MIPs in Figure 1C showed that these microparticles had spherical shape and rough surface with the average diameter of 300 nm. The inserted TEM micrograph in Figure 1C indicated that Fe_3O_4-β-CD@BAI-MIPs had a typical core-shell structure with a deep contrast inner core containing Fe_3O_4 nanoparticles and a slight contrast of MIP polymer shell. For comparisons, the molecularly imprinted polymer beads in absence of β-CD arm (Fe_3O_4@BAI-MIPs) were similarly prepared by precipitation polymerization of MAA functional monomer and EGDMA as crosslinker in presence of BAI as

template molecule and PEGylated Fe_3O_4 nanoparticles as core. The molecularly non-imprinted polymer beads in absence of BAI template (Fe_3O_4-β-CD@NIPs) were prepared by precipitation polymerization of MAA functional monomer and EGDMA as crosslinker with presence of PEGylated Fe_3O_4 nanoparticles as core.

The chemical structures of Fe_3O_4-β-CD@BAI-MIPs were confirmed by the FT-IR spectra in Figure 3. The presence of a peak at 2929 cm^{-1} in FT-IR spectrum of Fe_3O_4-β-CD@BAI-MIPs (Figure 3a) proved that the β-CD was incorporated in the imprinted polymer beads, which was consistent with that for the imprinted polymer using acryloyl-β-CD and acrylamide as functional monomers in the literature [28]. The presence of the peaks at 1728 cm^{-1} attributed to the stretching vibration of the carbonyl components from PMAA as well as PEGDMA network were clearly observed in Figures 3a,c,d for all these three polymer beads. The formation of P(EGDMA-*co*-MAA) shell-layer over Fe_3O_4 nanoparticles for Fe_3O_4-β-CD@BAI-MIPs and Fe_3O_4-β-CD@NIPs was attributed to the reaction between the tri-methoxy group from GPTMS and the hydroxyl groups of PEGylated magnetic nanoparticles, which was confirmed by Ji et al [29]. The P(EGDMA-*co*-MAA) shell-network in Fe_3O_4@BAI-MIPs was formed by ultrasonic assisted precipitation polymerization with the aid of efficient hydrogen-bonding interaction between the carboxyl group of PMAA and the hydroxyl group of the PEGylated Fe_3O_4 nanoparticles, which was similar to the construction of P(DVB-*co*-AA)@PAA@P(DVB-*co*-AA) (DVB: divinylbenzene) tri-layer microspheres in our previous work [30]. The peak ranging from 1630 to 1450 cm^{-1} in Figure 3a proved the incorporation of the BAI template molecules in Fe_3O_4-β-CD@BAI-MIPs, which was contributed from the stretching vibration of C-C bonds in BAI species. The strength for this wide peak was considerably decreased in Figure 3b after the extraction of the BAI with a mixture solvent of methanol and acetic acid (8/2, V/V) using soxhlet extraction technique, which confirmed the selective removal of the BAI templates from Fe_3O_4-β-CD@BAI-MIPs through the damage of hydrogen bonding interaction between the monomer and BAI.

Figure 3

The magnetic properties of the Fe_3O_4, Fe_3O_4@BAI-MIPs, Fe_3O_4-β-CD@BAI-MIPs, and Fe_3O_4-β-CD@BAI-NIPs were determined by VSM at room temperature in Figure 4. The saturation magnetization value of the particles was 15.99, 3.67, 2.43, and 2.0 emu/g, respectively.

The saturation magnetization values for the functionalized nanoparticles were significantly smaller than that for magnetite core nanoparticles, which was due to the considerable mass decrease of the neat magnetite species after the functionalization. No magnetic hysteresis loops were observed from the field dependent magnetization plots in Figure 4 for all these samples. In other words, the inexistence of remanence when magnetic field was removed, which implied that all the magnetic particles retained paramagnetic property originating from the magnetite core nanoparticles at room temperature. With the existence of an external magnetic field, the black suspension with these magnetic nanoparticles became transparent and clear within a short time. All these beads were attached to the walls of the vial as shown by the inserted digital photo in Figure 4. As a result, it would be possible to facilely separate these magnetic particles during the recovery of BAI recognition for these molecularly imprinted beads.

Figure 4

The amount of the inorganic components in Fe_3O_4, PEGylated Fe_3O_4, Fe_3O_4@BAI-MIPs, Fe_3O_4-β-CD@BAI-MIPs and Fe_3O_4-β-CD@NIPs were determined by TGA analyses as shown in Figure 5. These results demonstrated that the magnetite contents were 29.5 mass% for Fe_3O_4@MIPs, 19.3 mass% in Fe_3O_4-β-CD@BAI-MIPs and 16.1 mass% for Fe_3O_4-β-CD@NIPs, as the residual silica from β-CD was very low after pyrolysis of these hybrid beads. The significant decrease of magnetite content was consistent with the decrease of saturation magnetization value from 15.99 emu/g to 2.43 emu/g for these particles

Figure 5

Adsorption properties of the resultant polymer beads

A series of BAI standard solutions with concentrations of 0-5.0 mmol/L were utilized to determine the adsorption isotherms of these polymer beads via rolling the bottle for 24 h on a SHA-B shaker. The adsorption isotherms were illustrated in Figure 6. The amount of the adsorbed BAI was increased with increasing BAI concentration in the solution. For Fe_3O_4-β-CD@NIPs, the saturate adsorption capacity of 50 μmol/g was afforded with 2.0 mmol/L of BAI (Figure 6c). The adsorption of BAI for Fe_3O_4@MIPs increased with increasing the BAI concentration and reached a saturate adsorption capacity of 90 μmol/g at the BAI concentration of 3.0 mmol/L (Figure 6b). The adsorption of BAI for Fe_3O_4-β-CD@MIPs increased with enhancing the BAI concentration and reached a saturate adsorption capacity of 140 μmol/g at the BAI concentration of 4.0 mmol/L

(Figure 6a). The significant effect of imprinted BAI molecules in these systems attributed to the considerably higher adsorption capacities for Fe_3O_4-β-CD@MIPs (140 μmol/g, Figure 6a) and Fe_3O_4@MIPs (90 μmol/g) than that for Fe_3O_4-β-CD@NIPs (50 μmol/g). The synergic effect of the β-CD arm enhanced the imprinting efficiency for Fe_3O_4-β-CD@MIPs (140 μmol/g) with a much higher capactity than that for Fe_3O_4@MIPs (90 μmol/g) in absence of β-CD. Fe_3O_4-β-CD@NIPs had an adsorption capacity of 50 μmol/g, which may be due to the physical adsorption of BAI via the hydrogen bonding interaction between the carboxyl group of the polymer beads and the phenol group of BAI molecules.

Figure 6

A BAI standard solution with the concentration of 2.0 mmol/L was used to evaluate the dynamic adsorption for rebinding capacity of the resultant polymer beads. The adsorption dynamic curves of Fe_3O_4-β-CD@MIPs, Fe_3O_4@MIPs, Fe_3O_4-β-CD@NIPs were shown in Figure 7. It can be observed that the adsorption capacities of all these three beads increased very quickly at the first 20 min and then leveled off between 30 and 120 min. The adsorption equilibrium state was reached after 120 min. The results indicated that the adsorption capacities of Fe_3O_4-β-CD@MIPs (130 μmol/g) and Fe_3O_4@MIPs (100 μmol/g) were significant larger than that of Fe_3O_4-β-CD@NIPs (50 μmol/g). These were mainly attributed to the presence of the specific binding cavities, which were afforded by the selective removal of the templated BAI molecules from Fe_3O_4-β-CD@BAI-MIPs and Fe_3O_4@BAI-MIPs via Soxhlet extraction. Comparing to Fe_3O_4@MIPs, Fe_3O_4-β-CD@MIPs had a higher adsorption capacity via the incorporation of the β-CD arm in this system, which implied that more imprinted sites were well maintained during the extraction of BAI molecules due to the synergic effect of the silylated β-CD arm.

Figure 7

The adsorption kinetics of MIPs can be described via utilization of the internal diffusion model, the pseudo-first-order and pseudo second-order kinetic models [31, 32]. Through fitting the experimental data from Figure 6, the pseudo second-order model is better consistent with the kinetics of the adsorption characteristic of MIPs than those of the pseudo first-order according to the internal diffusion model. The kinetic data are calculated by the following formula according to the second-order model:

$$t/Q_t=1/(K_sQ_e^2)+(1/Q_e)*t \quad (5)$$

Where, the Q_e (μmol/g) and Q_t (μmol/g) represent the theory adsorption amounts and at time t (min), respectively. Ks ($g \cdot min^{-1} \cdot mmol^{-1}$) is the rate constant of the pseudo second-order.

The dynamic binding data were summarized in Table 1. These results indicated that the binding process could be the rate-limiting step for the whole adsorption process for BAI.

Table 1

The thermodynamics adsorption of Fe_3O_4-β-CD@MIPs was investigated under the temperature ranging from 293 to 333 K, which was treated by the thermodynamic equation:

$$\ln K_D = -\Delta_r G_m/RT = -\Delta_r H_m/RT + \Delta_r S_m/R \quad (6)$$

where, the K_D is the balance dissociation constant, $\Delta_r G_m$ (kJ/mol), $\Delta_r H_m$ (kJ/mol), and $\Delta_r S_m$ (J/K) are the Gibbs free energy, enthalpy and entropy change of the template molecules interacting with the binding sites of Fe_3O_4-β-CD@MIPs, respectively. The R is the molar gas constant. According to fitting the data by calculating from the Van't Hoff equation:

$$K_D = Q_e/C_e \quad (7)$$

The $\Delta_r H_m$ was -28.1 kJ/mol, which were obtained from the straight slope via plotting lnK_D and $10^3/T$ (Figure 8). This suggested that the process of imprinting adsorption was mainly via a physicochemical adsorption mechanism. The hydrogen-bonding interaction between the resultant polymers and BAI played as a driving force for the construction of Fe_3O_4-β-CD@MIPs.

Figure 8

The selectivity of Fe_3O_4-β-CD@MIPs, Fe_3O_4@MIPs, and Fe_3O_4-β-CD@NIPs was investigated by UV measurement of the residual amounts of BAI, Qu and non-analogue CAP in the upper liquid after the separation of the adsorbed beads via external magnetic field from the adsorption system. The adsorption was performed by adding independently these polymer beads into the solution of BAI, Qu and CAP with mild agitation on a SHA-B shaker for 20 h, respectively. The relevant data were summarized in Table 2. The selectivity factor of Fe_3O_4-β-CD@MIPs for Qu and CAP was 3.85 and 4.88, respectively. These results demonstrated that Fe_3O_4-β-CD@MIPs exhibited a higher selectivity for the adsorption of BAI templated molecules than those of Fe_3O_4@MIPs (2.56 and 2.94) and Fe_3O_4-β-CD@NIPs (1.16 and 1.20) for the reference molecules of Qu and CAP. The highest selectivity of Fe_3O_4-β-CD@MIPs was mainly contributed from the molecular size recognition via the hydrogen-bonding interaction between the BAI molecules and the carboxyl groups of PMAA with the synergic effect of β-CD

arm in Fe_3O_4-β-CD@MIPs comparing to that in Fe_3O_4@MIPs. The higher selectivity of BAI to CAP (4.85, 2.94) than that of BAI to Qu (3.85, 2.56) for the BAI-imprinted Fe_3O_4-β-CD@MIPs and Fe_3O_4@MIPs as chemical structure of Qu was more similar to that of BAI molecule. The selectivity of Fe_3O_4-β-CD@NIPs (1.16 and 1.20 to Qu and CAP) was very low as there were not specific cavities/sites left in the polymer network for the selective adsorption of BAI molecules with a very low saturate adsorption capacity (50 μmol/g).

Conclusion

In this study, Fe_3O_4-β-CD@MIPs core-shell microspheres were synthesized by sonic-irradiation assisted precipitation polymerization of MAA functional monomer and EGDMA as crosslinker in presence of BAI as imprinted molecules and the silylated β-CD-Fe_3O_4 nanoparticle as template. The β-CD played an essential role for the formation of a supramolecular monomer for precipitation polymerization via the hydrophobic interaction with BAI and the intra-molecular condensation with GPTMS. Comparing with the Fe_3O_4@MIPs and Fe_3O_4-β-CD@NIPs, the resultant Fe_3O_4-β-CD@MIPs incorporated with a β-CD arm had a unique selectivity for the adsorption of BAI molecules, the selectivity factor for Qu and CAP was 3.85 and 4.88, respectively. The results of the adsorption experiments indicated that such MIPs could selectively recognize the imprinting molecules. The imprinted process was accorded with second-order kinetic model, and was an exothermic reaction. In conclusion, the Fe_3O_4-β-CD@MIPs not only have the good selectivity and imprinting efficiency for BAI, but it also can be separated conveniently by external magnetic field and exhibit the super-paramagnetic behavior.

Acknowledgement

This work was supported by the National Natural Science Foundation of China (Grant Nos. 21174065 and 21374049), the Tianjin Municipal Natural Science Foundation (NO. 13JCQNJ C02600), and PCSIRT (IRT1257).

References

1 T. Nishioka, J. Kawabata, and Y. Aoyama, *J Nat Prod*, 1998, **61**:1413-1415.

2 D. S. Chou, G. Hsiao, Y. A. Lai, Y. J. Tsai, and J. R. Sheu, *Free Rad Bio Med*, 2009, **46**: 1197-1203.

3 J. A. Wu, A. S. Attele, L. Zhang, and C. S. Yuan, *Am J Chin Med*, 2001, **29**: 69-81.

4 H. Sun, Q. M. Che, X. Zhao, and X.P. Pu, *Eur J Pharm*, 2010, **631**: 53-60.

5 W. H. Chang, C. H. Chen, R. J. Gau, C. C. Lin, C. L. Tsai, K. Tsai, and F. J. Lu, *Planta Med*, 2002, **68**: 302-306.

6 Q. X. Zhang, J. Li, W. H. Zhang, X. P. Liao, and B. Shi, *Ind Eng Chem Res*, 2013, **52**: 2425-2433.

7 E. S. Ong, S. M. Len, *Anal Chim Acta*, 2003, **482**: 81-89.

8 B. Gao , Y. Li, and Z. J. Zhang, *J Chromatogr B*, 2010, **878**: 2077-2086.

9 K. Matsumoto, A. Torimaru, S. Ishitobi, T. Sakai, H. Ishikawa, K. Toko, N. Miura, and T. Imato, *Talanta,* 2005, **68**: 305-311.

10 H. J. Wang, W. H. Zhou, X. F. Yin, Z. X. Zhuang, H. H. Yang, and X. R. Wang, *J Am Chem Soc,* 2006, **128**: 15954-15955.

11 F. G. Tamayo, E. Turiel, and A. Martín-Esteban , *J Chromatogr A*, 2007, **1152**: 32-40.

12 K. Haupt, and K. Mosbach, *Chem Rev*, 2000, **100**: 2495-2504.

13 V. Pichon, and F. Chapuis-Hugon, *Anal Chim Acta*, 2008, **622**: 48-61.

14 J. P. Lai, X. Y. Lu, C. Y. Lu, H. F. Ju, and X. W. He, *Anal Chim Acta,* 2001, **442**: 105-111.

15 R. X. Gao, X. Kong, X. Wang, X. W. He, L. X. Chen, Y. K. Zhang, *J Mater Chem*, 2011, 21, 17863-17871.

16 Y. Zhang, Y. W. Li, Y. L. Hu, G. K. Li, and Y. Q. Chen, *J Chromatogr A*, 2010, **1217**: 7337-7344.

17 E. Schneiderman, A. M. Stalcup, *J Chrom B Biomed Sci Appl*, 2000, 745: 83-102.

18 A. G. Strikovsky, D. Kasper, M.Grün, B. S. Green, J. Hradil, and G. Wulff, J. Am. Chem. Soc, 2000, **122**, 6295-6296.

19 A. G. Mayes, K. Mosbach, *Anal Chem*, 1996, **68**, 3769-3774.

20 N. Pérez, M. J. Whitcombe, E. N. Vulfson, *J Appl Polym Sci*, 2000, **77**, 1851-1859.

21 J. S. Downey, G. McIsaac, R. S. Frank, and H. D. H. Stöver, *Macromolecules,* 2001, **34**, 4534-4541.

22 F. Bai, X. L. Yang, and W. Q. Huang, *Macromolecules*, 2004, **37**: 9746-9752.

23 N. Phutthawong, M. Pattarawarapan. *Polym bull*, 2013, **70**, 691-705.

24 B. Y. Zu, G. Q. Pan, X. Z. Guo, Y. Zhang, and H. Q. Zhang, *J Polym Sci Poly Chem*, 2009, **47**: 3257-3270.

25 Y. Y. Zheng, X. B. Wang, L. Shang, C. R. Li, C. Cui, W. J. Dong, W. H. Tang, B. Y. Chen, *Mater Charact*, 2010, **61**: 489-492.

26 C. T. Rao, B. Lindberg, J. Lindberg, and J. Pitha, *J Org Chem*, 1991, **56**: 1327-1329.

27 L. Qin, X. W. He, W. Y. Li, and Y. K. Zhang, *J Chromatogr A*, 2008, **1187**: 94-102.

28 W. Zhang, L. Qin, X. W. He, W. Y. Li, and Y. K. Zhang, *J Chromatogr A*, 2009, **1216**: 4560-4567.

29 Y. S. Ji, X. Y. Liu, M. Guan, C. D. Zhao, H. Y. Huang, H. X. Zhang, and C. M. Wang, *J Sep Sci*, 2009, **32**: 2139-2145.

30 G. L. Li, and X. L. Yang, *J Phys Chem B*, 2007, **111**: 12781-12786.

31 E. Demirbas, M. Kobya, E. Senturk, and T. Ozkan, *Water Sa*, 2004. **30**: 533-539.

32 Y. S.Ho, and G. McKay, *Process Bioch*, 1999, **34**: 451-465.

Captions to Scheme, Figures, and Tables

Scheme 1 Synthesis of Fe_3O_4-β-CD@BAI-MIPs

Figure 1 FESEM and TEM micrograph of A) Fe_3O_4 nanoparticles; B) PEGylated Fe_3O_4 nanoparticles; C) Fe_3O_4-β-CD@BAI-MIPs.

Figure 2 The UV-spectra of A) BAI/MAA, B) BAI/β-CD, C) BAI/MAA/β-CD with different molar ratios in DMF solution.

Figure 3 FT-IR spectra: a) Fe_3O_4-β-CD@BAI-MIPs; b) Fe_3O_4-β-CD@MIPs; c) Fe_3O_4@MIPs; d) Fe_3O_4-β-CD@NIPs.

Figure 4 Magnetic properties by VSM technique: a) Fe_3O_4 nanoparticles; b) Fe_3O_4@MIPs; c) Fe_3O_4-β-CD@BAI-MIPs; d) Fe_3O_4-β-CD@NIPs.

Figure 5 TGA curves: a) Fe_3O_4 nanoparticles; b) PEGylated Fe_3O_4 nanoparticles; c) Fe_3O_4@BAI-MIPs; d) Fe_3O_4-β-CD@BAI-MIPs; e) Fe_3O_4-β-CD@NIPs

Figure 6 Adsorption isotherms of BAI on functional beads: a) Fe_3O_4-β-CD@MIPs; b) Fe_3O_4@MIPs; c) Fe_3O_4-β-CD@NIPs.

Figure 7 Dynamic adsorption of BAI on functional polymer beads: a) Fe_3O_4-β-CD@MIPs; b) Fe_3O_4@MIPs; c) Fe_3O_4-β-CD@NIPs.

Figure 8 The relationship between the dissociate equilibrium constant and temperature for the adsorption of BAI on Fe_3O_4-β-CD@MIPs

Table 1 The dynamic binding indexes for the adsorption of BAI on the functional polymer beads

Table 2 The selectivity of BAI for the adsorption of BAI on the functional polymer beads

Scheme 1

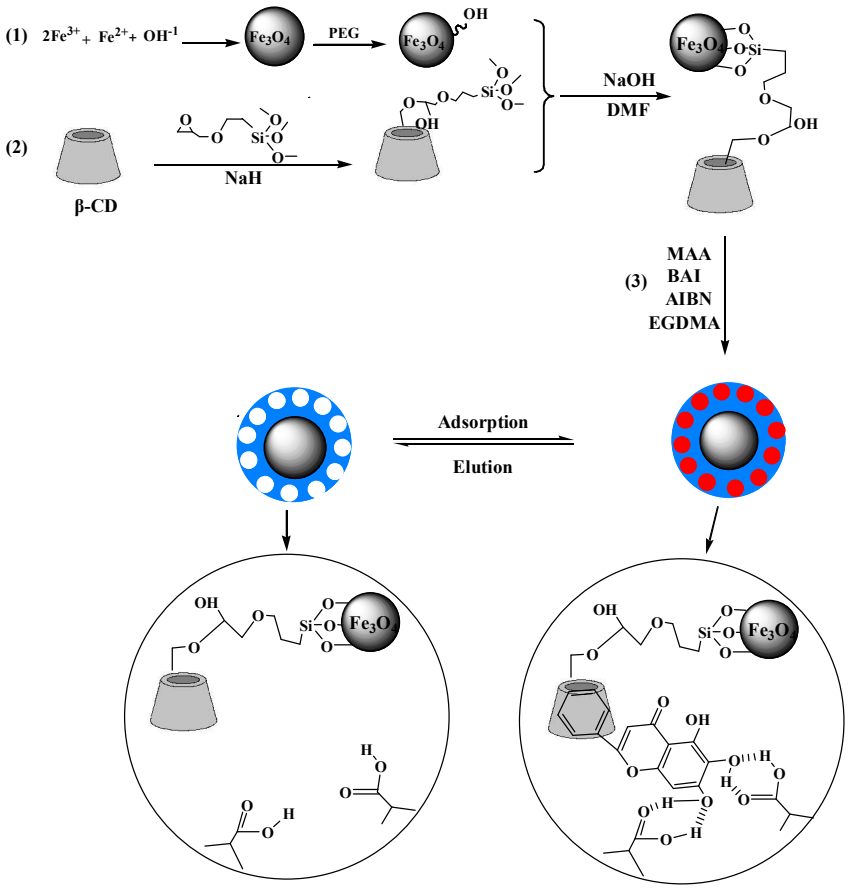

Figure 1

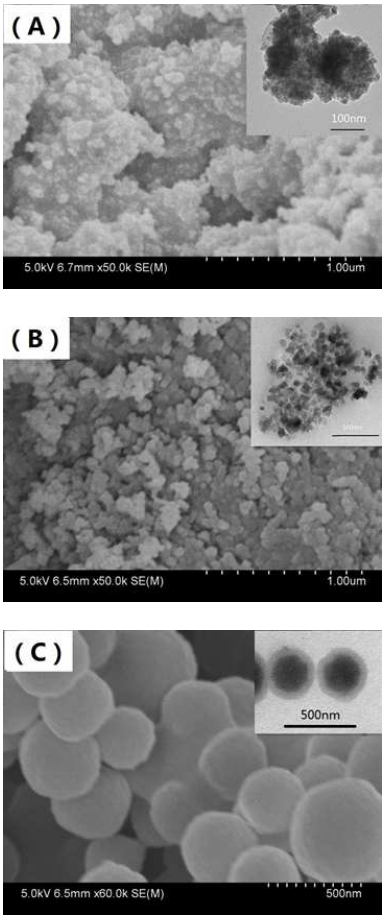

Figure 2

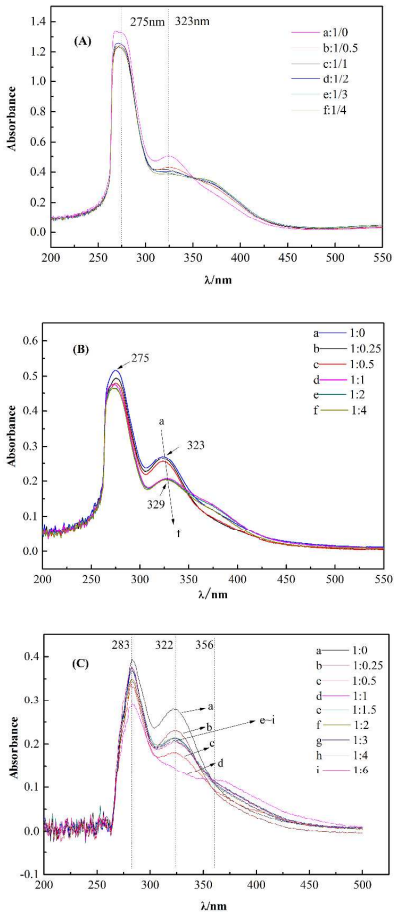

Figure 3

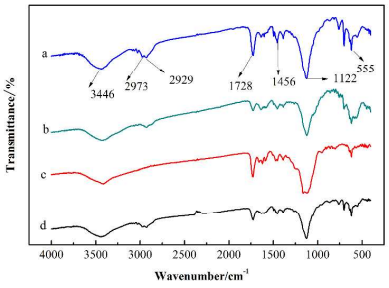

Figure 4

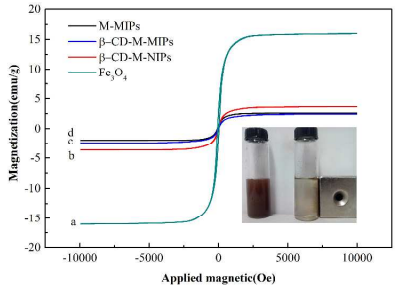

Figure 5

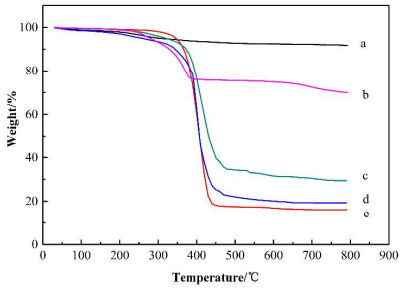

Figure 6

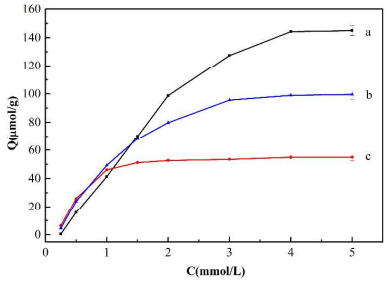

Figure 7

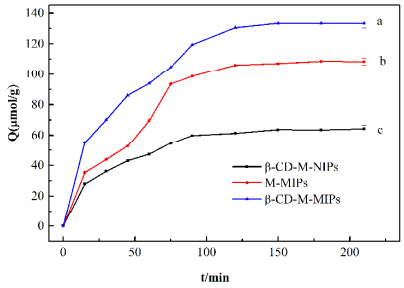

Figure 8

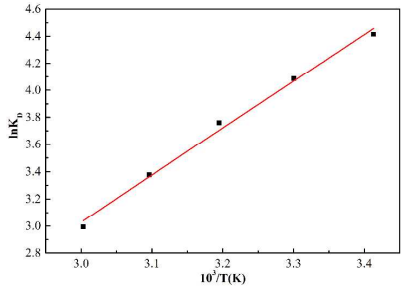

Table 1

Beads	Equation	Q_e	Q_t	K_s	R^2
Fe_3O_4-β-CD@MIPs	$t/Q_t=0.0073t+0.3441$	137.3	133.5	0.00015	0.9949
Fe_3O_4@MIPs	$t/Q_t=0.0091t+0.0698$	110.2	108.5	0.00119	0.9967
Fe_3O_4-β-CD@NIPs	$t/Q_t=0.0146t+0.3186$	68.6	64.2	0.00067	0.9990

Table 2

Substance	Fe_3O_4-β-CD@MIPs				Fe_3O_4@MIPs				Fe_3O_4-β-CD@NIPs		
	Q	K_d	α	β	Q	K_d	α	β	Q	K_d	α
BAI	133.5	201	1.00	2.08	108	118.5	1.0	1.69	64	47.31	1.00
Qu	68.5	52	3.85	1.18	63	46.3	2.56	1.10	58	40.65	1.16
CAP	58.1	401	4.88	1.03	57	40.3	2.94	1.02	56	39.31	1.20